Appl. Math. Mech. -Engl. Ed., **45**(2), 277–294 (2024)

APPLIED MATHEMATICS AND MECHANICS (ENGLISH EDITION)

https://doi.org/10.1007/s10483-024-3076-8

Tuning mechanical behaviors of highly entangled hydrogels with the random distribution of mobile entanglements*

Jinlong LIU[1], Di LU[1,2], Bin CHEN[3,4,†]

1. Department of Engineering Mechanics, Zhejiang University, Hangzhou 310027, China;
2. Beijing System Design Institute of Electro-Mechanic Engineering, Beijing 100854, China;
3. Intelligent Robotic Research Center, Zhejiang Laboratory, Hangzhou 310027, China;
4. Key Laboratory of Soft Machines and Smart Devices of Zhejiang Province, Hangzhou 311100, China

(Received Nov. 3, 2023 / Revised Dec. 11, 2023)

Abstract Highly entangled hydrogels exhibit excellent mechanical properties, including high toughness, high stretchability, and low hysteresis. By considering the evolution of randomly distributed entanglements within the polymer network upon mechanical stretches, we develop a constitutive theory to describe the large stretch behaviors of these hydrogels. In the theory, we utilize a representative volume element (RVE) in the shape of a cube, within which there exists an averaged chain segment along each edge and a mobile entanglement at each corner. By employing an explicit method, we decouple the elasticity of the hydrogels from the sliding motion of their entanglements, and derive the stress-stretch relations for these hydrogels. The present theoretical analysis is in agreement with experiment, and highlights the significant influence of the entanglement distribution within the hydrogels on their elasticity. We also implement the present developed constitutive theory into a commercial finite element software, and the subsequent simulations demonstrate that the exact distribution of entanglements strongly affects the mechanical behaviors of the structures of these hydrogels. Overall, the present theory provides valuable insights into the deformation mechanism of highly entangled hydrogels, and can aid in the design of these hydrogels with enhanced performance.

Key words highly entangled hydrogel, constitutive theory, entanglement, gamma distribution

Chinese Library Classification O34, O21, O411
2010 Mathematics Subject Classification 74A20, 74D10

* Citation: LIU, J. L., LU, D., and CHEN, B. Tuning mechanical behaviors of highly entangled hydrogels with the random distribution of mobile entanglements. *Applied Mathematics and Mechanics* (*English Edition*), **45**(2), 277–294 (2024) https://doi.org/10.1007/s10483-024-3076-8

† Corresponding author, E-mail: chenb6@zju.edu.cn

Project supported by the Key Research Project of Zhejiang Laboratory (No. K2022NB0AC03), the National Natural Science Foundation of China (No. 11872334), and the National Natural Science Foundation of Zhejiang Province of China (No. LZ23A020004)

1 Introduction

Conventional hydrogels typically exhibit weak and fragile mechanical properties[1]. To overcome these limitations, various strategies and methods were implemented to synthesize hydrogels with high mechanical performance[2–6]. By carefully designing their microstructures, hydrogels can be fabricated with both high toughness and large stretchability at a high water content[7]. With the combination of two polymer networks, double-network hydrogels partially addressed the trade-off between stiffness and toughness and exhibited exceptional mechanical strength[8–9], although they often displayed pronounced hysteresis[8,10]. Recently, highly entangled hydrogels containing dense entanglements within their polymer networks have emerged as a promising solution to the stiffness-toughness confliction while also displaying low hysteresis, friction, and wear resistance[10]. The superb mechanical properties of highly entangled hydrogels have spurred significant research efforts exploring their applications in advanced hydrogel adsorbents, fatigue-resistant adhesives, low-friction coatings and so on[11–15].

Though the roles of physical entanglements, as well as chemical crosslinks, within polymer networks were investigated through experimental and phenomenological approaches[16–18], there have been limited efforts to study the physical mechanisms of entanglements from a micromechanical perspective[19]. Additionally, the development of theoretical models for hydrogels incorporating the effects of entanglements remains inadequate[20], despite the existence of various constitutive theories proposed to study different behaviors of hydrogels[21–27]. It is crucial and enticing to model the mechanical behaviors of highly entangled hydrogels by considering mobile entanglements from the molecular level up.

There appears to exist significant similarity between highly entangled hydrogels and synthetic slide-ring hydrogels[3], both of which contain sliding crosslinks. The slide-ring hydrogels also display excellent mechanical properties, including high extensibility, low viscosity, and high toughness[3]. By considering molecular frictions induced by sliding of rings on polymer chains, a nonaffine constitutive theory for large stretch behaviors of these hydrogels was developed[28]. The analysis based on the theory clearly indicated that sliding of rings was critical for their high fracture energy, which helped provide insights into understanding high mechanical performance of slide-ring hydrogels. However, in modeling the large stretch behaviors of slide-ring gels[28], all polymer chains within the slide-ring gel networks were assumed to have the same contour length. Such an idealized assumption may not accurately capture the real mechanical response of the gel networks of highly entangled hydrogels[10].

Entanglements within highly entangled hydrogels can be randomly distributed, which would result in randomly distributed contour lengths of chain segments separated by entanglements. It is known that the distribution of chain contour lengths within polymer networks, occurring naturally during polymerization, significantly influences the mechanical behavior of soft materials[29–30], which is crucial for constitutive models to account for[30]. Various assumptions regarding the distribution of polymer chain contour lengths were proposed in modeling the mechanical behavior of polymer materials. These included the classical Gaussian pattern[31–32], the uniform distribution[30,33–35], the log-normal distribution[30,35–37], the exponential distribution[30,38–39], the Dirac delta distribution[30,35], the Weibull distribution[30,35], and the normal distribution[30,35]. Exploring how randomly distributed entanglements within highly entangled hydrogels affect their mechanical behaviors is an intriguing issue.

To address this issue, we develop a cross-scale constitutive theory for highly entangled hydrogels by considering the random distribution of contour lengths of polymer chain segments separated by randomly distributed entanglements. In our theory, we account for the sliding motion of randomly distributed mobile entanglements within the polymer chain network. We characterize the distribution evolution of contour lengths of chain segments within the network using a specific statistical distribution, namely the gamma distribution, which allows us to capture the nonuniform nature of contour length of polymer chain segment within the hydrogel.

We use our theory to predict the stress response of highly entangled hydrogels under uniaxial tension and compare the results with experimental data. Further, we implement the theory into the ABAQUS/explicit finite element program using a vectorized user-material (VUMAT) subroutine. This enables us to study the mechanical behaviors of structures made of highly entanglement hydrogels under complex loading conditions. Our analysis demonstrates that the presence of a high density of randomly distributed entanglements can effectively alleviate stress through sliding mechanisms, and the exact distribution of entanglements significantly affects the mechanical behaviors of structures of these hydrogels. We anticipate that our theory provides insights into understanding the excellent mechanical performance of highly entangled hydrogels.

2 Theory

Entanglements greatly outnumber crosslinks within the polymer network of a highly entangled hydrogel[10]. As schematically illustrated in Fig. 1(a), there exist a significant number of mobile entanglements along each polymer chain within the gel, which would separate the polymer chain into multiple chain segments with varied contour lengths. The presence of these mobile entanglements would allow for sliding of chain segments subject to mechanical loads or swelling due to water absorption, as illustrated in Fig. 1(a).

In the theory, the gel at the dry state is represented with a representative volume element (RVE) of a cube, as illustrated in Fig. 1(b). Within the RVE, there exists one chain segment along each edge of the cube and a mobile entanglement at each corner of the cube. Each chain segment within the cube represents the averaged behavior of numerous chain segments within the gel. Within the RVE, the edges of the cube always coincide with the principal directions of stretches.

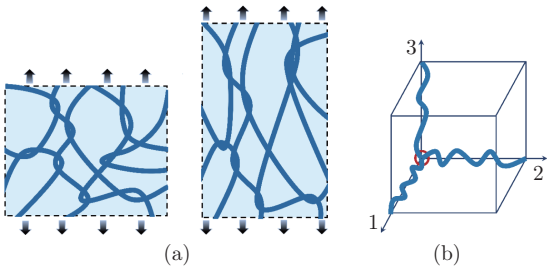

Fig. 1 (a) The schematic of a highly entangled hydrogel with dense entanglements, where entanglements within hydrogels function as mobile crosslinks, which can slide along polymer chains when hydrogels are subject to mechanical loading or water swelling; (b) the RVE of the hydrogel with dense entanglements, where there exists a chain segment along each edge of the cube and a mobile entanglement (red ring) at each corner of the cube (color online)

The initial dimension of the cube is l_0, corresponding to the initial length of a chain segment within the RVE at the dry state, which can be related to the contour length of the chain segment at the dry state, denoted as $\overline{L}_{\mathrm{C0}}$, through[40]

$$l_0 = \sqrt{2\xi \overline{L}_{\mathrm{C0}}}, \tag{1}$$

where ξ is the persistence length. Note that the contour lengths of three chain segments within the RVE at the dry state are exactly the same. When the RVE is deformed due to water absorption or mechanical loads, its current dimensions along three principal directions would change, denoted as l_1, l_2, and l_3, respectively. With the consideration of volume conservation, we have[41]

$$l_1 l_2 l_3 = l_0^3 + \Omega M, \tag{2}$$

where Ω is the volume per water molecule, and M is the number of absorbed water molecules.

At the current time, the principal stretches of the RVE, denoted as λ_i, are given by $\lambda_i = l_i/l_0$. With Eq. (2), we have

$$\lambda_1\lambda_2\lambda_3 = 1 + \Omega C, \tag{3}$$

where $C = M/l_0^3$ is the nominal concentration of water.

The force-stretch relationship of a chain segment within the RVE is described by the worm-like chain theory[42],

$$F = \frac{k_{\mathrm{B}}T}{\xi}\Big(\frac{1}{4}\Big(1 - \frac{x}{L_{\mathrm{C}}}\Big)^{-2} - \frac{1}{4} + \frac{x}{L_{\mathrm{C}}}\Big), \tag{4}$$

where k_{B} denotes the Boltzmann constant, T is the absolute temperature, x is its displacement of one end with respect to the other end, and L_{C} is its contour length.

When chain segments in the RVE are unequal in forces, they would slide relatively to entanglements so that their respective contour length changes. This sliding may also affect the effective number density of chain segments within gels, as will be considered later. With an explicit method[28], we decouple the elasticity of the gel from chain segment sliding within the gel. At the current time t, contour lengths of three chain segments in the RVE are assumed to be fixed, which are only updated in the duration between neighboring steps Δt.

We solve the elastic field of the gel by employing the principle of virtual work[43–44]. Let the RVE at the current time change its dimensions by infinitesimal small amounts δl_1, δl_2, and δl_3. Simultaneously, the number of absorbed water molecules within the RVE changes, which leads to the change in the virtual work done by the chemical potential of water, denoted as μ, being $\mu\delta M$. Hence, the change in the internal energy within the RVE, denoted as δu, should fulfil

$$\delta u = \sigma_1 l_2 l_3 \delta l_1 + \sigma_2 l_3 l_1 \delta l_2 + \sigma_3 l_1 l_2 \delta l_3 + \mu\delta M, \tag{5}$$

where σ_1, σ_2, and σ_3 denote the three principal stresses, respectively. With Eqs. (2) and (5), we have

$$\delta u = \Big(\sigma_1 + \frac{\mu}{\Omega}\Big) l_0^3 \lambda_2\lambda_3\delta\lambda_1 + \Big(\sigma_2 + \frac{\mu}{\Omega}\Big) l_0^3 \lambda_3\lambda_1\delta\lambda_2 + \Big(\sigma_3 + \frac{\mu}{\Omega}\Big) l_0^3 \lambda_1\lambda_2\delta\lambda_3. \tag{6}$$

At the current time, we also have

$$\delta u = \frac{\partial u}{\partial \lambda_1}\delta\lambda_1 + \frac{\partial u}{\partial \lambda_2}\delta\lambda_2 + \frac{\partial u}{\partial \lambda_3}\delta\lambda_3. \tag{7}$$

With Eqs. (6) and (7), also considering that $\delta\lambda_1$, $\delta\lambda_2$, and $\delta\lambda_3$ are arbitrary and independent variables, we have

$$\begin{cases} \sigma_1 = \dfrac{1}{\lambda_2\lambda_3}\dfrac{\partial U}{\partial \lambda_1} - \dfrac{\mu}{\Omega}, \\ \sigma_2 = \dfrac{1}{\lambda_3\lambda_1}\dfrac{\partial U}{\partial \lambda_2} - \dfrac{\mu}{\Omega}, \\ \sigma_3 = \dfrac{1}{\lambda_1\lambda_2}\dfrac{\partial U}{\partial \lambda_3} - \dfrac{\mu}{\Omega}, \end{cases} \tag{8}$$

where $\delta U (= \delta u/l_0^3)$ denotes the change in the internal energy density within the RVE.

The change in the internal energy density within the RVE due to the change in the principal stretches is the sum of the change in the elastic energy density of polymer chains, denoted as U_1, and that in the energy density of mixing water with polymers, denoted as U_2. Thus, we have

$$\delta U = \delta U_1 + \delta U_2. \tag{9}$$

In Eq. (9),

$$\delta U_1 = N_1\delta\varepsilon_1 + N_2\delta\varepsilon_2 + N_3\delta\varepsilon_3, \tag{10}$$

where $N_i\,(i = 1, 2, 3)$ denotes the effective number density of chain segments along the ith principal direction, and $\varepsilon_i\,(i = 1, 2, 3)$ denotes the elastic energy stored within the chain segment along the ith principal direction. The elastic energy stored within one chain segment is given by $\varepsilon = \int F\mathrm{d}x$. The energy density of mixing water with polymers is given by[41]

$$U_2 = k_{\mathrm{B}}T\Big(C\ln\frac{\Omega C}{1+\Omega C} + \frac{\chi C}{1+\Omega C}\Big), \tag{11}$$

where χ is a measure of the interactions between polymer chains and water. Note that the effect of the presence of crosslinks between chains is not accounted for in Eq. (11).

With Eqs. (8)–(11), we have

$$\begin{cases} \sigma_1 = \dfrac{N_1F_1l_0}{\lambda_2\lambda_3} + \dfrac{k_{\mathrm{B}}T}{\Omega}\Big(\ln\Big(1-\dfrac{1}{\lambda_1\lambda_2\lambda_3}\Big) + \dfrac{1}{\lambda_1\lambda_2\lambda_3} + \dfrac{\chi}{\lambda_1^2\lambda_2^2\lambda_3^2}\Big) - \dfrac{\mu}{\Omega}, \\ \sigma_2 = \dfrac{N_2F_2l_0}{\lambda_3\lambda_1} + \dfrac{k_{\mathrm{B}}T}{\Omega}\Big(\ln\Big(1-\dfrac{1}{\lambda_1\lambda_2\lambda_3}\Big) + \dfrac{1}{\lambda_1\lambda_2\lambda_3} + \dfrac{\chi}{\lambda_1^2\lambda_2^2\lambda_3^2}\Big) - \dfrac{\mu}{\Omega}, \\ \sigma_3 = \dfrac{N_3F_3l_0}{\lambda_1\lambda_2} + \dfrac{k_{\mathrm{B}}T}{\Omega}\Big(\ln\Big(1-\dfrac{1}{\lambda_1\lambda_2\lambda_3}\Big) + \dfrac{1}{\lambda_1\lambda_2\lambda_3} + \dfrac{\chi}{\lambda_1^2\lambda_2^2\lambda_3^2}\Big) - \dfrac{\mu}{\Omega} \end{cases} \tag{12}$$

with the detailed derivation given in Appendix A.

With the explicit method, we only consider sliding of chain segments in the duration between neighboring time steps. The sliding velocity of chain segments within the RVE is given by

$$V_{ij} = \frac{F_i - F_j}{\eta}, \tag{13}$$

where $i \neq j$, V_{ij} denotes the sliding velocity of the jth chain segment towards the ith chain segment, F_i corresponds to the force of the ith chain segment, and η is a linear frictional coefficient between polymer chains and entanglements, which is set to be a very small value so as not to induce any vincible viscosity in the analysis. As shown in Appendix A, the choice of Eq. (13) would make our constitutive theory consistent with the 2nd law of thermodynamics.

With Eq. (13), the changes in the contour lengths of three chain segments within the RVE during Δt, denoted as $\Delta\overline{L}_{\mathrm{C1}}$, $\Delta\overline{L}_{\mathrm{C2}}$, and $\Delta\overline{L}_{\mathrm{C3}}$, respectively, are given by

$$\begin{cases} \Delta\overline{L}_{\mathrm{C1}} = (V_{12} + V_{13})\Delta t, \\ \Delta\overline{L}_{\mathrm{C2}} = (V_{21} + V_{23})\Delta t, \\ \Delta\overline{L}_{\mathrm{C3}} = (V_{31} + V_{32})\Delta t. \end{cases} \tag{14}$$

Note that each chain segment within the RVE represents the averaged behavior of numerous chain segments within the gel. The contour lengths of these chain segments within the gel are generally non-uniform with a random distribution depending on the fabrication procedure. Upon sliding, the contour lengths of chain segments within the gel would change. When a chain segment becomes too short, i.e., neighboring entanglements on its two sides become too close, entanglements would merge so that the chain segment would vanish. On the other hand, merged entanglements could re-emerge due to chain sliding so that a new chain segment would be born. Such a phenomenon would affect the effective number density of chain segments within the gel.

To calculate the effective number density of chain segments within the gel at $t + \Delta t$, we consider that the initial contour lengths of chain segments separated by entanglements along each principal direction at the dry state, denoted as y, are randomly distributed. Without

losing its generality, y is assumed to follow the gamma distribution, given by

$$f(y)=\frac{1}{\beta^{\alpha}\Gamma(\alpha)}y^{\alpha-1}\exp\Big(-\frac{y}{\beta}\Big), \tag{15}$$

where f is the probability density function of y, α is the shape parameter of the gamma distribution, and β is the scale parameter of the gamma distribution. Since y is always positive, we would have

$$\int_0^{+\infty}\frac{1}{\beta^{\alpha}\Gamma(\alpha)}y^{\alpha-1}\exp\Big(-\frac{y}{\beta}\Big)\mathrm{d}y=1. \tag{16}$$

With the probability density function described by Eq. (15), the averaged contour length of these chain segments would be $\alpha\beta$, which is taken as the contour length of chain segment within the RVE at the dry state. It is further assumed that chain sliding does not affect the shape parameter of α but affects the scale parameter of β in Eq. (15) for the random distribution of contour lengths of chain segments along each principal direction at $t+\Delta t$. This assumption might be justified with the consideration of Eq. (4), where the stretch and the force of the chain segment are one-to-one match. When regarding that chain segments along one principal direction within the gel have the same stretch and the same force at t, the same scaling of their contour lengths during Δt would still yield the same chain forces at $t+\Delta t$. In this way, we will have

$$\begin{cases}\beta_1^{t+\Delta t}=\overline{L}_{\mathrm{C1}}^{t+\Delta t}/\alpha,\\ \beta_2^{t+\Delta t}=\overline{L}_{\mathrm{C2}}^{t+\Delta t}/\alpha,\\ \beta_3^{t+\Delta t}=\overline{L}_{\mathrm{C3}}^{t+\Delta t}/\alpha,\end{cases} \tag{17}$$

where $\overline{L}_{\mathrm{C1}}^{t+\Delta t}$, $\overline{L}_{\mathrm{C2}}^{t+\Delta t}$, and $\overline{L}_{\mathrm{C3}}^{t+\Delta t}$ correspond to the respective contour lengths of three chain segments within the RVE at $t+\Delta t$, and $\beta_1^{t+\Delta t}$, $\beta_2^{t+\Delta t}$, and $\beta_3^{t+\Delta t}$ correspond to respective scale parameters of the gamma distribution for chain segments within the gel along the principal directions at $t+\Delta t$.

When a chain segment within the gel becomes too short, for example, $\sim$1 nm, neighboring entanglements would strongly interact with each other. The complex formed by this very short chain segment and neighboring entanglements can have a relatively high stiffness. In our opinion, the force on chain segments is more or less equal within the highly entangled hydrogels so that a relatively small amount of elastic energy would be stored within such a complex. For this reason, we have not included this tiny amount of elastic energy in the model. However, these chains are not moved away from the model system. If they become long again due to chain sliding, their elastic energy would be re-counted in the model. Specifically, a chain segment within the gel is counted in calculating the effective number density of chain segment only when its current contour length is above a critical small value, denoted as L_{cr}. The effective number densities of chain segments along the three principal directions at $t+\Delta t$, denoted as $N_1^{t+\Delta t}$, $N_2^{t+\Delta t}$, and $N_3^{t+\Delta t}$, are given by

$$\begin{cases}N_1^{t+\Delta t}=\dfrac{N_0}{3}\Big(1-\displaystyle\int_0^{L_{\mathrm{cr}}}\frac{1}{\beta_1{}^{\alpha}\Gamma(\alpha)}x^{\alpha-1}\exp\Big(-\frac{x}{\beta_1}\Big)\mathrm{d}x\Big),\\ N_2^{t+\Delta t}=\dfrac{N_0}{3}\Big(1-\displaystyle\int_0^{L_{\mathrm{cr}}}\frac{1}{\beta_2{}^{\alpha}\Gamma(\alpha)}x^{\alpha-1}\exp\Big(-\frac{x}{\beta_2}\Big)\mathrm{d}x\Big),\\ N_3^{t+\Delta t}=\dfrac{N_0}{3}\Big(1-\displaystyle\int_0^{L_{\mathrm{cr}}}\frac{1}{\beta_3{}^{\alpha}\Gamma(\alpha)}x^{\alpha-1}\exp\Big(-\frac{x}{\beta_3}\Big)\mathrm{d}x\Big),\end{cases} \tag{18}$$

respectively, where N_0 is the number density of chain segments within the gel.

There exist fixed crosslinks with a relatively low density within highly entangled hydrogels, which would provide constraints on the total contour length of chain segments within the gel network and help prevent the gel from collapsing. We have enforced that the total contour lengths of polymer chain segments within the RVE are conserved upon loading in the theory. Thus, with Eq. (18), to keep total contour lengths of polymer chains along each principal direction within the gel conserved, the effective contour lengths of three chain segments within the RVE at $t+\Delta t$, denoted as $\widetilde{L}_{\mathrm{C1}}^{t+\Delta t}$, $\widetilde{L}_{\mathrm{C2}}^{t+\Delta t}$, and $\widetilde{L}_{\mathrm{C3}}^{t+\Delta t}$, which would be used in the calculation of Eq. (12), are given by

$$\begin{cases} \widetilde{L}_{\mathrm{C1}}^{t+\Delta t} = \dfrac{N_0 \overline{L}_{\mathrm{C1}}^{t+\Delta t}}{3N_1^{t+\Delta t}}, \\ \widetilde{L}_{\mathrm{C2}}^{t+\Delta t} = \dfrac{N_0 \overline{L}_{\mathrm{C2}}^{t+\Delta t}}{3N_2^{t+\Delta t}}, \\ \widetilde{L}_{\mathrm{C3}}^{t+\Delta t} = \dfrac{N_0 \overline{L}_{\mathrm{C3}}^{t+\Delta t}}{3N_3^{t+\Delta t}}. \end{cases} \tag{19}$$

Due to entanglement sliding, the contour length between neighboring entanglements would change so that the corresponding end-to-end distance for the chain segment between neighboring entanglements without force would also change, given by

$$\begin{cases} \Delta l_{01} = \sqrt{2\xi \widetilde{L}_{\mathrm{C1}}} - \sqrt{2\xi \overline{L}_{\mathrm{C0}}}, \\ \Delta l_{02} = \sqrt{2\xi \widetilde{L}_{\mathrm{C2}}} - \sqrt{2\xi \overline{L}_{\mathrm{C0}}}, \\ \Delta l_{03} = \sqrt{2\xi \widetilde{L}_{\mathrm{C3}}} - \sqrt{2\xi \overline{L}_{\mathrm{C0}}}, \end{cases} \tag{20}$$

respectively, where Δl_{01}, Δl_{02}, and Δl_{03} denote the changes in the corresponding end-to-end distance for the chain segment between neighboring entanglements without force within the RVE. The displacements of each chain segment within the RVE, denoted as x_1, x_2, and x_3, would then be

$$\begin{cases} x_1 = (\lambda_1 - 1) l_0 - \Delta l_{01}, \\ x_2 = (\lambda_2 - 1) l_0 - \Delta l_{02}, \\ x_3 = (\lambda_3 - 1) l_0 - \Delta l_{03}. \end{cases} \tag{21}$$

We will use the constitutive theory developed above to predict large stretch behaviors of highly entangled hydrogels in the following. In all analyses, $\sigma_1 = \sigma_2 = \sigma_3 = 0$ at the free swelling state with $\lambda_1 = \lambda_2 = \lambda_3 = \lambda_{\mathrm{s}}$. The stretches in the analyses are then normalized by λ_{s}. The strain rate, denoted as γ, is given by $\gamma = \frac{\Delta\lambda_1}{\lambda_{\mathrm{s}}\Delta t}$, with $\Delta\lambda_1$ being the change in λ_1 within a time step of Δt. Default values of parameters used in the analysis are listed in Table 1.

Table 1 Default parameters in the simulations

Item	Parameter	Item	Parameter
N_0	$0.204\,\mathrm{nm}^{-3}$	$k_{\mathrm{B}}T$	$4.01\,\mathrm{pN}\cdot\mathrm{nm}$
L_{cr}	$1.3\,\mathrm{nm}$	Ω	$0.03\,\mathrm{nm}^3$[41]
η	$0.000\,1\,\mathrm{pN}\cdot\mathrm{s}\cdot\mathrm{nm}^{-1}$[28]	μ	0[41]
χ	0.01[28]	ξ	$0.35\,\mathrm{nm}$[28]

3 Effects of entanglement distribution on the stress-stretch curves of highly entangled gels

With Eq. (15), the effects of α or β for the initial distribution of contour lengths of chain

segments within the gel are displayed in Fig. 2. In Figs. 2(a) and 2(b), when $\alpha = 0.5$ or $\alpha = 1$, the probability density function monotonically decreases as the contour length gets larger. Note that, when $\alpha = 1$, the gamma distribution will be exactly the exponential distribution. In Fig. 2(c), when $\alpha = 5$, the probability density function becomes unimodal, which increases and then decreases as the contour length gets larger. Since the mean value of the gamma distribution is given by $\alpha\beta$, and its variance is given by $\alpha\beta^2$, both the mean value and the variance become greater as β gets larger with fixed α in Figs. 2(a)–2(c).

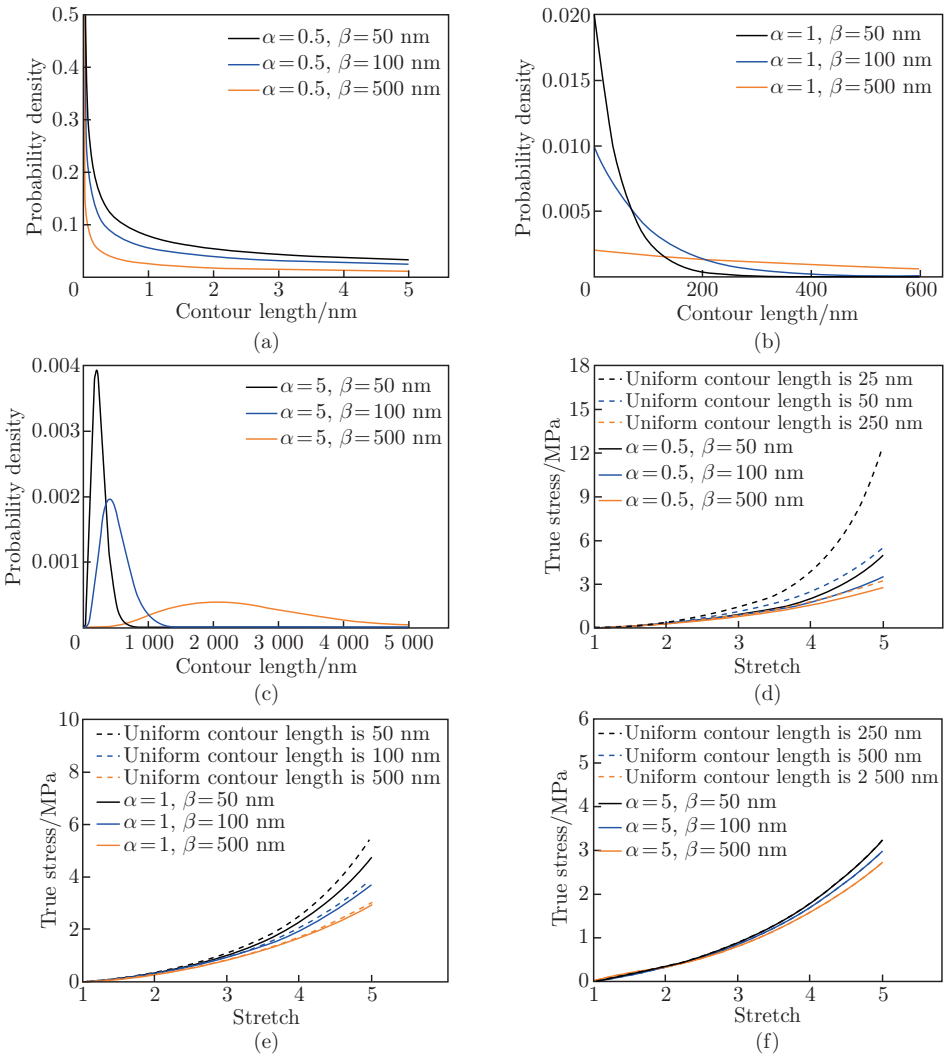

Fig. 2 (a)–(c) The effects of α or β in gamma distribution on the probability density of initial contour lengths of polymer chain segments within the gel; (d)–(f) theoretical predictions of stress-stretch curves of the corresponding gel. Predictions for the cases with uniform initial contour lengths are also plotted for comparison (color online)

With varied initial distributions of contour lengths of chain segments within the gel displayed in Figs. 2(a)–2(c), we use the developed constitutive theory to predict stress-stretch curves of the corresponding gel. In the analysis, the gel is under uniaxial tension. The predictions are displayed in Figs. 2(d)–2(f), where the stress generally increases with the stretch. In Figs. 2(d)–2(f), the stress is lower as β gets larger at the same stretch with fixed α. This result is reasonable,

since, with fixed α, the larger β is, the larger the initial contour lengths of chain segments would be, and thus the gel becomes softer. For comparison, the predicted stress-stretch curves for the gel with uniform initial contour lengths of chain segments are also plotted in Figs. 2(d)–2(f), with its stress being generally larger than that of the gamma distribution. The predicted stress-stretch curve for the gel with uniform initial contour lengths of chain segments almost coincides with that with the gamma distribution when $\alpha = 5$. As β gets larger, the predicted stress-stretch curve for the gel with uniform initial contour lengths of chain segments will also get closer to that with the gamma distribution. These results can be understood. With the gamma distribution, there will be a portion of chain segments with the contour length, which is smaller than $L_{\rm cr}$, leading to a lower effective chain number. In this way, the predicted stress-stretch curve for the gel with uniform initial contour lengths of chain segments should be harder than that with the gamma distribution. As seen in Fig. 2(c), when $\alpha = 5$, there exist only a very small portion of chain segments with the contour length smaller than $L_{\rm cr}$, and thus the predicted stress-stretch curve for the gel with uniform initial contour lengths of chain segments is almost the same as that with the gamma distribution.

We also investigate the case when the mean value of $\alpha\beta$ is fixed, with results displayed in Fig. 3. With fixed $\alpha\beta$, when α becomes larger, β would become smaller, and the variance of $\alpha\beta^2$ would also become smaller. As inferred from Figs. 3(a)–3(c), the portion of chain segments with initial contour lengths, which are smaller than $L_{\rm cr}$, decreases as α gets larger. Under this condition, the effective number of chain segments within the corresponding gel would be higher. Therefore, as displayed in Figs. 3(d)–3(f), the stress-stretch curves get higher as α gets larger. For comparison, the predicted stress-stretch curves for the gel with uniform initial contour lengths of chain segments are also plotted in Figs. 3(d)–3(f), with its stress being generally larger than that of the gamma distribution.

4 Predictions of the stress-stretch curves of synthesized highly entangled gels

With our developed theory, we then make predictions of the stress-stretch curves of synthesized highly entangled gels[10], as displayed in Fig. 4. Parametrical values are carefully chosen to be physically sound in our analysis. For example, the chain density in the analysis is calculated based on the initial elastic modulus reported in the experiment[10]. The average of the initial contour length of chain segments in the experiments was estimated to be about 50 nm[10], while that used in our analysis is 39 nm. The gamma distribution employed in the prediction is displayed in Fig. 4(a). As seen in Fig. 4(b), when $\alpha = 1$ and $\beta = 39$ nm, our prediction of the stress-stretch curve of the synthesized gels upon uniaxial tension agrees quite well with the experiment[10]. Such good agreement may also suggest the validity of our choice of gamma distribution in developing the constitutive theory in this work.

In Fig. 4(c), the evolution of effective number density of chain segments with the stretch within the gel is presented. As clearly seen in Fig. 4(c), the effective number density of chain segments along the stretch direction gradually gets larger upon uniaxial tension, because merged entanglements re-emerge due to chain sliding, and new chain segments are re-born. Meanwhile, the effective number density of chain segments perpendicular to the stretch direction gradually gets smaller, because entanglements would merge, and chain segments would temporarily disappear when a chain segment becomes too short due to chain sliding. In Fig. 4(d), the evolution of the contour length of chain segment within the RVE with the stretch is presented, which clearly shows that the contour length of chain segment along the stretch direction within the RVE gets longer, which appears to saturate at relatively large stretches, while that perpendicular to the stretch direction gets shorter, which almost approaches 0.

We further validate our model by comparing theoretical predictions with other experimental data in the literature. In Fig. 5(a), we simulate the stress-stretch curve of a highly entangled

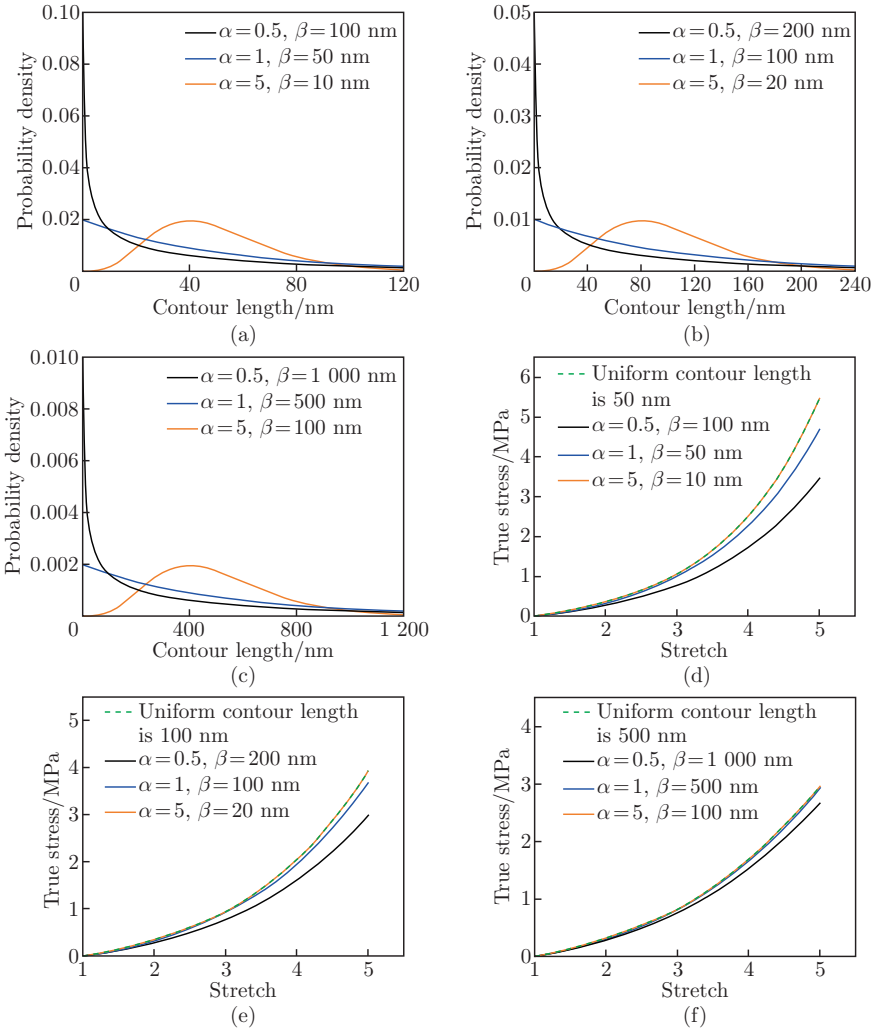

Fig. 3 (a)–(c) The effects of the product of $\alpha\beta$ in gamma distribution on the probability density of initial contour lengths of polymer chain segments within hydrogels; (d)–(f) theoretical predictions of stress-stretch curves of hydrogels under uniaxial tension with varied distributions of entanglements within hydrogels. Predictions for the case with uniform initial contour lengths are also plotted for comparison (color online)

elastomer containing limited amount of water under uniaxial extension[10]. In the analysis, we have set $\chi = 0.6$ to make the free swelling ratio λ_s small enough. As illustrated in Fig. 5(a), our model prediction can capture the stress-stretch response of a highly entangled elastomer[10]. In Figs. 5(b) and 5(c), we also predict the stress-stretch curves under uniaxial loading of other synthetic highly entangled hydrogels as reported in Refs. [11] and [45], which agree well with the experiment.

As displayed in Figs. 6(a) and 6(b), our model can also predict rate independence and the negligible hysteresis of highly entangled hydrogels, which agrees with the experiment[10]. However, the experiment[10] also showed that the as-prepared highly entangled hydrogels with a low water content can exhibit pronounced hysteresis, which can also be predicted by our model, as shown in Fig. 6(c). Note that the frictional coefficient is set to be $0.000\,1\,\mathrm{pN}\cdot\mathrm{s}\cdot\mathrm{nm}^{-1}$ for our analysis displayed in Figs. 6(a) and 6(b), but a relatively large value of $0.12\,\mathrm{pN}\cdot\mathrm{s}\cdot\mathrm{nm}^{-1}$ for that displayed in Fig. 6(c).

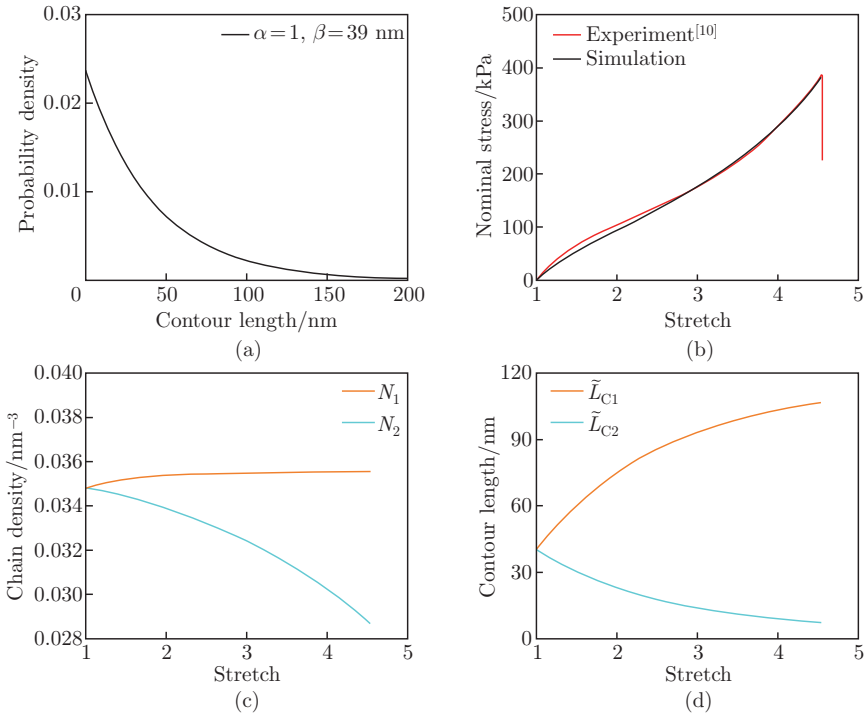

Fig. 4 (a) The predicted probability density of initial contour lengths of polymer chain segments within hydrogels; (b) the theoretical prediction of the stress-stretch curve agrees with the experimental results[10]; (c) the effective number of chain segments along the loading direction increases slowly while decreases rapidly along the perpendicular direction of the loading with stretch; (d) the average contour length along the loading direction increases and that perpendicular to the loading direction decreases with stretch. In the simulation, $\alpha = 1$, $\beta = 39\,\mathrm{nm}$, the initial effective number of chain segments is $0.108\,\mathrm{nm}^{-3}$, and the stretch rate is $0.025\,\mathrm{s}^{-1}$ (color online)

5 Analysis of structures made of highly entangled gels upon complex loading conditions

To facilitate the prediction of mechanical behaviors of structures made of highly entangled hydrogels subject to complex loading conditions, we further implement the developed constitutive theory into the ABAQUS through a VUMAT subroutine. In our numerical scheme, a second-order tensor $\boldsymbol{L}_{\mathrm{C}}$ is utilized, defined as

$$\boldsymbol{L}_{\mathrm{C}} = \begin{pmatrix} \overline{L}_{\mathrm{C1}} & & \\ & \overline{L}_{\mathrm{C2}} & \\ & & \overline{L}_{\mathrm{C3}} \end{pmatrix} \tag{22}$$

with $L_{\mathrm{C}}^{\mathrm{total}} = \overline{L}_{\mathrm{C1}} + \overline{L}_{\mathrm{C2}} + \overline{L}_{\mathrm{C3}}$ being the first invariant of $\boldsymbol{L}_{\mathrm{C}}$. The tensor components within $\boldsymbol{L}_{\mathrm{C}}$ are initially set in the principal axes of isotropic stretches at the free swelling state. In complex deformations, we set the off-diagonal components of $\boldsymbol{L}_{\mathrm{C}}$ to be 0, and only three diagonal components of $\boldsymbol{L}_{\mathrm{C}}$ will be updated during a time interval of Δt.

With the programmed VUMAT subroutine, we simulate the stress field of a plate with a circular hole existing at its center upon uniaxial tensional stretches, as illustrated in Fig. 7(a). Several types of gel materials are under our investigation, i.e., the contour length of chain segments within gels follows the gamma distribution with mobile entanglements, the contour length of chain segments within gels follows the gamma distribution but with fixed crosslinks,

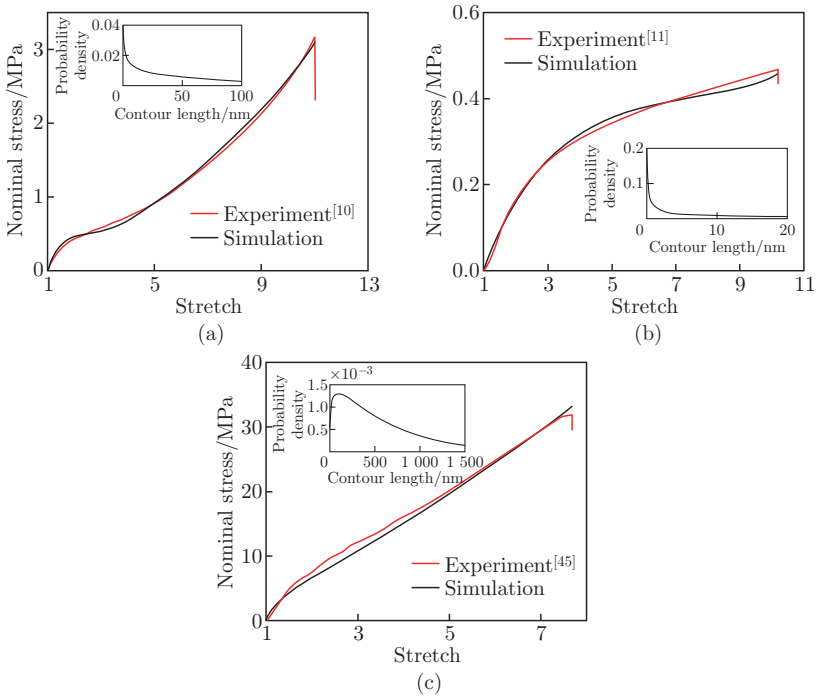

Fig. 5 Comparison of our model predictions with other experimental data: (a) the stress-stretch curve of a highly entangled elastomer under uniaxial tension[10], where in the analysis, $N_0 = 0.249\,\mathrm{nm}^{-3}$, $\alpha = 0.7$, $\beta = 128.57\,\mathrm{nm}$, $\eta = 0.4\,\mathrm{pN}\cdot\mathrm{s}\cdot\mathrm{nm}^{-1}$, and $\chi = 0.6$; (b) the stress-stretch curve of a highly entangled hydrogel under uniaxial tension[11], where in the analysis, $N_0 = 0.075\,\mathrm{nm}^{-3}$, $\alpha = 0.3$, $\beta = 1\,667\,\mathrm{nm}$, $\eta = 11\,\mathrm{pN}\cdot\mathrm{s}\cdot\mathrm{nm}^{-1}$, $L_{\mathrm{cr}} = 0.1\,\mathrm{nm}$, and $\chi = 0.45$; (c) a stress-stretch curve of a highly entangled hydrogel under uniaxial tension[45], where in the analysis, $N_0 = 0.008\,4\,\mathrm{nm}^{-3}$, $\alpha = 1.2$, $\beta = 500\,\mathrm{nm}$, $\eta = 0.000\,8\,\mathrm{pN}\cdot\mathrm{s}\cdot\mathrm{nm}^{-1}$, and $\chi = 0.48$ (color online)

and the initial contour length of chain segments within gels is uniform with mobile entanglements. Simulation results are presented in Figs. 7(b) and 7(c). The maximum of the nominal stress, σ_{11}, which occurs at the top of the hole, increases with the stretch, as displayed in Fig. 7(b). The case with fixed crosslinks shows the largest value, the case with the uniform contour length is the second largest, and the case with the gamma distribution is the smallest. The contours of the von Mises stress at the same stretch for three different gel materials are also displayed in Fig. 7(c), where we can clearly see that the sliding of entanglements dramatically lowers the stress concentration near the hole. We can also see that the exact random distribution of entanglements within highly entangled gels significantly affects the mechanical behaviors of complex structures made of them.

6 Discussion

In the classical theories of rubber elasticity, such as the 3-chain model[46] or the 8-chain model[47], it is assumed that the edges of the unit cell of the RVE always align with the directions of principal stretches. Following this tradition, we also assume that the chain segment orientations within the RVE always align with the principal stretch directions in the theory. Note that, at each material point, the gel is represented with a unit cell with chain segments oriented in three orthogonal directions. However, under complex loading conditions, the unit cell for each material point within the gel structure may have different rotations or deformations with different cuboidal shapes.

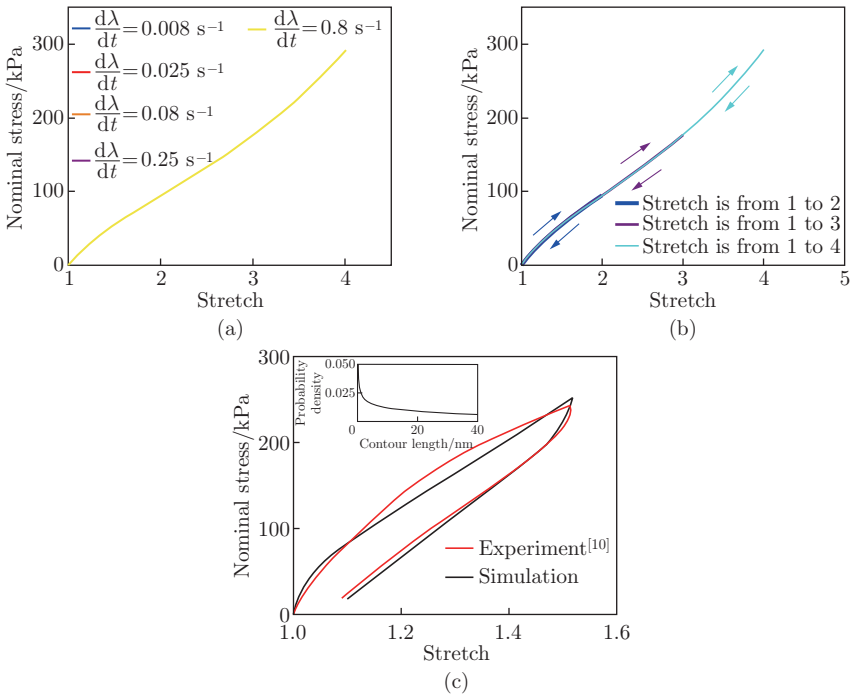

Fig. 6 (a) The prediction of the rate independence for the fully swollen highly entangled hydrogel, where in the analysis, $\eta = 0.000\,1\,\mathrm{pN{\cdot}s{\cdot}nm^{-1}}$; (b) the prediction of the negligible hysteresis for the fully swollen highly entangled hydrogel, where arrows indicate loading or unloading, and $\eta = 0.000\,1\,\mathrm{pN\cdot s\cdot nm^{-1}}$; (c) the prediction of the pronounced hysteresis for the as-prepared highly entangled hydrogel, where in the analysis, $\eta = 0.12\,\mathrm{pN\cdot s\cdot nm^{-1}}$ (color online)

The behavior of each chain segment within the RVE represents the average behavior of many chain segments with the contour length distribution within hydrogels. It is possible to calculate the average force over the contour length distribution when these chain segments are subject to the same compatible stretch and then take it as the force acting on a chain segment within the RVE. However, using this routine approach may result in significant differences in the force between chain segments with different contour lengths. In our opinion, within highly entangled hydrogels, the forces within chain segments are more or less equal before reaching the sliding limit. To address this issue in our theory, we instead average the contour length over the contour length distribution. Subsequently, we calculate the force for each chain segment within the RVE based on the force-stretch relationship. It is important to note that conserving the contour length of chain segments within highly entangled hydrogels is critical in developing our theory.

Within highly entangled hydrogels, entanglements would impose constraints on the available entropic configurations of chain segment fluctuations, which should be weaker than those imposed by physical or chemical bonds. In this context, we approximate these entanglements as sliding constraints. However, we must admit that there may potentially be additional degrees of freedom at entanglement sites. For example, two chains wrapped around each other as a double helix can unwrap under certain load combinations or thermal fluctuations, termed as the de-twisting mode. If there is a de-twisting mode existing between chain segments, it could result in a sudden change in the available length for entropic fluctuation, rather than the gradual change assumed in our current work that focuses solely on the sliding mode.

Such a de-twisting mode may exhibit similarities to folded domains within protein chains, where the unfolding of folded domains upon loads would also result in a sudden change in the available length for entropic fluctuation. As seen from the previous studies[48], a sudden change

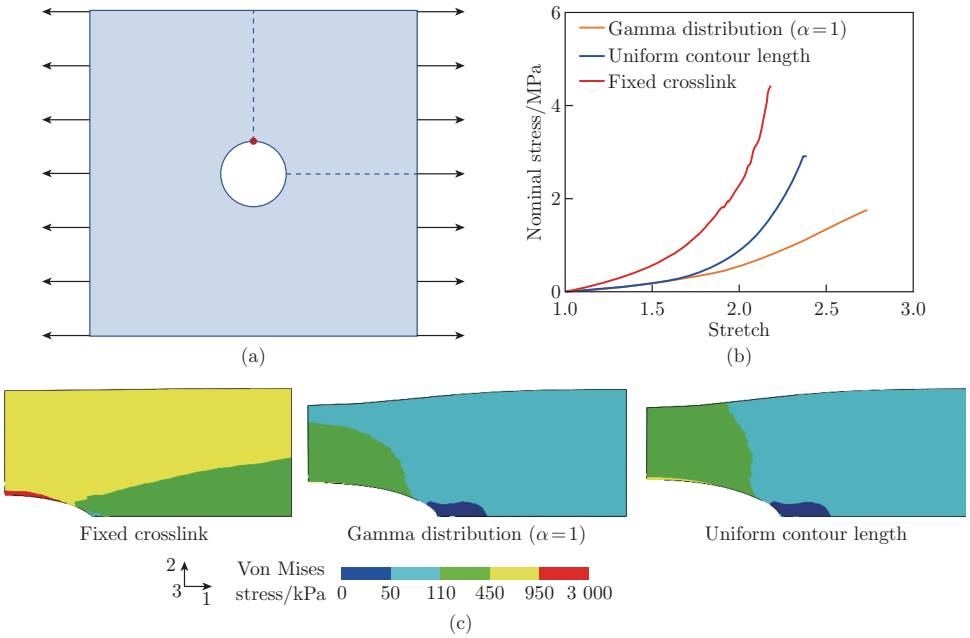

Fig. 7 Stresses in a plate with a circular hole existing at its center upon uniaxial tension, where three types of gel materials are under investigation, and the gel with fixed crosslinks is the stiffest, followed by the one with the uniform contour length, and then the one with the gamma distribution: (a) schematic of a square plate with a circular hole at its center subject to uniaxial tension; (b) the maximum of the nominal stress, σ_{11}, within the plate changes with stretch; (c) stress contours at a stretch ratio of 2. In the simulations, the initial contour length of the chain segments within the RVE is 39 nm, the number density of chain segments is $0.108\,\mathrm{nm}^{-3}$, the stretch rate is $0.1\,\mathrm{s}^{-1}$, the critical value of the contour length for the case with the uniform contour length is 0, and other parameters are listed in Table 1 by default. For the case of fixed crosslinks, the frictional coefficient is set to be a very large value, which is $10\,000\,\mathrm{pN}\cdot\mathrm{s}\cdot\mathrm{nm}^{-1}$ (color online)

in the polymer chain contour length within protein hydrogels upon loading can lead to significant energy dissipation. However, experimental findings have demonstrated that highly entangled hydrogels exhibit negligible energy dissipation and fully recoverable stress-stretch curves during cyclic loading. If de-twisting occurs in highly entangled hydrogels under loading conditions, re-twisting would be expected to take place. This process would lead to a considerable amount of energy dissipation, which contradicts the observed experimental results. As a result, we speculate that the occurrence of the de-twisting mode in highly entangled hydrogels during loading is relatively low, even if it exists.

7 Conclusions

In this study, we develop a constitutive theory for highly entangled hydrogels based on the random distribution of entanglements within them. Our analysis indicates that the developed model is able to predict mechanical behaviors of highly entangled hydrogels well. We also implement this theory into the ABAQUS/explicit using a user subroutine of VUMAT. We find that a high density of mobile entanglements can play a crucial role in transmitting force along polymer chains and effectively relieving stresses caused by applied loads. Our analysis also indicates that the exact distribution of entanglements strongly affects the mechanical behaviors of structures of these hydrogels. We believe that this theory provides a constructive approach for quantitatively designing highly entangled hydrogels with exceptional properties.

Conflict of interest The authors declare no conflict of interest.

References

[1] GUO, X., DONG, X. Y., ZOU, G. J., GAO, H. J., and ZHAI, W. Strong and tough fibrous hydrogels reinforced by multiscale hierarchical structures with multimechanisms. *Science Advances*, **9**(2), eadf7075 (2023)

[2] HUA, M. T., WU, S. W., MA, Y. F., ZHAO, Y. S., CHEN, Z. L., FRENKEL, I., STRZALKA, J., ZHOU, H., ZHU, X. Y., and HE, X. M. Strong tough hydrogels via the synergy of freeze-casting and salting out. *nature*, **590**(7847), 594–599 (2021)

[3] LIU, C., MORIMOTO, N., JIANG, L., KAWAHARA, S., NORITOMI, T., YOKOYAMA, H., MAYUMI, K., and ITO, K. Tough hydrogels with rapid self-reinforcement. *Science*, **372**(6546), 1078–1081 (2021)

[4] NIAN, G. D., KIM, J., BAO, X. Y., and SUO, Z. G. Making highly elastic and tough hydrogels from doughs. *Advanced Materials*, **34**(50), 2206577 (2022)

[5] WANG, Z., ZHENG, X. J., OUCHI, T., KOUZNETSOVA, T. B., BEECH, H. K., AV-RON, S., MATSUDA, T., BOWSER, B. H., WANG, S., JOHNSON, J. A., KALOW, J. A., OLSEN, B. D., GONG, J. P., RUBINSTEIN, M., and CRAIG, S. L. Toughening hydrogels through force-triggered chemical reactions that lengthen polymer strands. *Science*, **374**(6564), 193–196 (2021)

[6] ZHAO, X. H., CHEN, X. Y., YUK, H., LIN, S. T., LIU, X. Y., and PARADA, G. Soft materials by design: unconventional polymer networks give extreme properties. *Chemical Reviews*, **121**(8), 4309–4372 (2021)

[7] HAN, S. J., WU, Q. R., ZHU, J. D., ZHANG, J. Y., CHEN, A. B., SU, S., LIU, J. T., HUANG, J. R., YANG, X. X., and GUAN, L. H. Tough hydrogel with high water content and ordered fibrous structures as an artificial human ligament. *Materials Horizons*, **10**(3), 1012–1019 (2023)

[8] GONG, J. P., KATSUYAMA, Y., KUROKAWA, T., and OSADA, Y. Double-network hydrogels with extremely high mechanical strength. *Advanced Materials*, **15**(14), 1155–1158 (2003)

[9] JIA, Y. T., ZHOU, Z. D., JIANG, H. L., and LIU, Z. S. Characterization of fracture toughness and damage zone of double network hydrogels. *Journal of the Mechanics and Physics of Solids*, **169**, 105090 (2022)

[10] KIM, J., ZHANG, G. G., SHI, M. X. Z., and SUO, Z. G. Fracture, fatigue, and friction of polymers in which entanglements greatly outnumber cross-links. *Science*, **374**(6564), 212–216 (2021)

[11] LI, D. K., ZHAN, W., ZUO, W., LI, L. P., ZHANG, J., CAI, G. Y., and TIAN, Y. Elastic, tough and switchable swelling hydrogels with high entanglements and low crosslinks for water remediation. *Chemical Engineering Journal*, **450**, 138417 (2022)

[12] LIU, P. Y., ZHANG, Y., GUAN, Y., and ZHANG, Y. J. Peptide-crosslinked, highly entangled hydrogels with excellent mechanical properties but ultra-low solid content. *Advanced Materials*, **35**(13), 2210021 (2023)

[13] SHI, M. X. Z., KIM, J., NIAN, G. D., and SUO, Z. G. Highly entangled hydrogels with degradable crosslinks. *Extreme Mechanics Letters*, **59**, 101953 (2023)

[14] WANG, Y. C., NIAN, G. D., KIM, J., and SUO, Z. G. Polyacrylamide hydrogels VI: synthesis-property relation. *Journal of the Mechanics and Physics of Solids*, **170**, 105099 (2023)

[15] TANI, J., TAKAGI, T., and QIU, J. Intelligent material systems: application of functional materials. *Applied Mechanics Reviews*, **51**(8), 505–521 (1998)

[16] BOSNJAK, N. and SILBERSTEIN, M. N. Pathways to tough yet soft materials. *Science*, **374**(6564), 150–151 (2021)

[17] BUKOWSKI, C., ZHANG, T., RIGGLEMAN, R. A., and CROSBY, A. J. Load-bearing entanglements in polymer glasses. *Science Advances*, **7**(38), eabg9763 (2021)

[18] ZHU, J. K. and LUO, J. Effects of entanglements and finite extensibility of polymer chains on the mechanical behavior of hydrogels. *Acta Mechanica*, **229**, 1703–1719 (2018)

[19] EDWARDS, S. F. and VILGIS, T. The effect of entanglements in rubber elasticity. *Polymer*, **27**(4), 483–492 (1986)

[20] NIAN, X. C., YANG, Q. S., MA, L. H., and ZHANG, X. Y. Constitutive modeling for hydrogel with chain entanglements and application to adaptive hydrogel composite structures. *Mechanics of Advanced Materials and Structures*, **30**(24), 5122–5136 (2023)

[21] BAYAT, M. R., DOLATABADI, R., and BAGHANI, M. Transient swelling response of ph-sensitive hydrogels: a monophasic constitutive model and numerical implementation. *International Journal of Pharmaceutics*, **577**, 119030 (2020)

[22] BÖGER, L., NATEGHI, A., and MIEHE, C. A minimization principle for deformation-diffusion processes in polymeric hydrogels: constitutive modeling and FE implementation. *International Journal of Solids and Structures*, **121**, 257–274 (2017)

[23] MENG, Q. H. and SHI, X. H. A mechanistically motivated constitutive model of biopolymer hydrogels with structural evolution. *Journal of the Mechanics and Physics of Solids*, **173**, 105205 (2023)

[24] HUANG, R., ZHENG, S. J., LIU, Z. S., and NG, T. Y. Recent advances of the constitutive models of smart materials — hydrogels and shape memory polymers. *International Journal of Applied Mechanics*, **12**(2), 2050014 (2020)

[25] PAN, Z. Z. and BRASSART, L. Constitutive modelling of hydrolytic degradation in hydrogels. *Journal of the Mechanics and Physics of Solids*, **167**, 105016 (2022)

[26] WANG, Q. M. and GAO, Z. M. A constitutive model of nanocomposite hydrogels with nanoparticle crosslinkers. *Journal of the Mechanics and Physics of Solids*, **94**, 127–147 (2016)

[27] DAL, H., AÇIKGÖZ, K., and BADIENIA, Y. On the performance of isotropic hyperelastic constitutive models for rubber-like materials: a state of the art review. *Applied Mechanics Reviews*, **73**(2), 020802 (2021)

[28] LU, D. and CHEN, B. A constitutive theory for large stretch behaviors of slide-ring gels by considering molecular frictions. *Soft Matter*, **19**(8), 1531–1539 (2023)

[29] FALENDER, J. R., YEH, G. S. Y., and MARK, J. E. The effect of chain length distribution on elastomeric properties 1: comparisons between random and highly nonrandom networks. *Journal of the American Chemical Society*, **101**(24), 7353–7356 (1979)

[30] LI, B. and BOUKLAS, N. A variational phase-field model for brittle fracture in polydisperse elastomer networks. *International Journal of Solids and Structures*, **182-183**, 193–204 (2020)

[31] DARGAZANY, R. and ITSKOV, M. A network evolution model for the anisotropic Mullins effect in carbon black filled rubbers. *International Journal of Solids and Structures*, **46**(16), 2967–2977 (2009)

[32] ZHANG, H. H. and HU, Y. H. A statistical-chain-based theory for dynamic living polymeric gels with concurrent diffusion, chain remodeling reactions and deformation. *Journal of the Mechanics and Physics of Solids*, **172**, 105155 (2023)

[33] GHAREEB, A. and ELBANNA, A. An adaptive quasicontinuum approach for modeling fracture in networked materials: application to modeling of polymer networks. *Journal of the Mechanics and Physics of Solids*, **137**, 103819 (2020)

[34] LAVOIE, S. R., LONG, R., and TANG, T. Modeling the mechanics of polymer chains with deformable and active bonds. *The Journal of Physical Chemistry B*, **124**(1), 253–265 (2020)

[35] WANG, Q. M., GOSSWEILER, G. R., CRAIG, S. L., and ZHAO, X. H. Mechanics of mechanochemically responsive elastomers. *Journal of the Mechanics and Physics of Solids*, **82**, 320–344 (2015)

[36] GUO, Q. and ZAÏRI, F. A micromechanics-based model for deformation-induced damage and failure in elastomeric media. *International Journal of Plasticity*, **140**, 102976 (2021)

[37] LU, T. Q., WANG, Z. T., TANG, J. D., ZHANG, W. L., and WANG, T. J. A pseudo-elasticity theory to model the strain-softening behavior of tough hydrogels. *Journal of the Mechanics and Physics of Solids*, **137**, 103832 (2020)

[38] ITSKOV, M. and KNYAZEVA, A. A rubber elasticity and softening model based on chain length statistics. *International Journal of Solids and Structures*, **80**, 512–519 (2016)

[39] YASUDA, Y., MASUMOTO, T., MAYUMI, K., TODA, M., YOKOYAMA, H., MORITA, H., and ITO, K. Molecular dynamics simulation and theoretical model of elasticity in slide-ring gels. *ACS Macro Letters*, **9**(9), 1280–1285 (2020)

[40] TRELOAR, L. R. G. The elasticity and related properties of rubbers. *Reports on Progress in Physics*, **36**(7), 755 (1973)

[41] CAI, S. Q. and SUO, Z. G. Mechanics and chemical thermodynamics of phase transition in temperature-sensitive hydrogels. *Journal of the Mechanics and Physics of Solids*, **59**(11), 2259–2278 (2011)

[42] MARKO, J. F. and SIGGIA, E. D. Statistical mechanics of supercoiled DNA. *Physical Review E*, **52**(3), 2912–2938 (1995)

[43] EPSTEIN, M. and SEGEV, R. Differentiable manifolds and the principle of virtual work in continuum mechanics. *Journal of Mathematical Physics*, **21**(5), 1243–1245 (2008)

[44] LÁNCZOS, C. *The Variational Principles of Mechanics*, Courier Corporation, U. S. A. (2012)

[45] NORIOKA, C., INAMOTO, Y., HAJIME, C., KAWAMURA, A., and MIYATA, T. A universal method to easily design tough and stretchable hydrogels. *NPG Asia Materials*, **13**(1), 34 (2021)

[46] JAMES, H. M. and GUTH, E. Theory of the elastic properties of rubber. *The Journal of Chemical Physics*, **11**(10), 455–481 (1943)

[47] ARRUDA, E. M. and BOYCE, M. C. A three-dimensional constitutive model for the large stretch behavior of rubber elastic materials. *Journal of the Mechanics and Physics of Solids*, **41**(2), 389–412 (1993)

[48] FAN, Q. Y., CHEN, B., and CAO, Y. Constitutive model reveals the defect-dependent viscoelasticity of protein hydrogels. *Journal of the Mechanics and Physics of Solids*, **125**, 653–665 (2019)

Appendix A

(I) The detailed derivation of Eq. (12)

With Eq. (10), we will have

$$\delta U_1 = N_1 F_1 l_0 \delta\lambda_1 + N_2 F_2 l_0 \delta\lambda_2 + N_3 F_3 l_0 \delta\lambda_3. \tag{A1}$$

With Eq. (11), we will have

$$\delta U_2 = k_{\mathrm{B}} T \delta\Big(C \ln \frac{\Omega C}{1+\Omega C} + \frac{\chi C}{1+\Omega C} \Big). \tag{A2}$$

With Eq. (A2), we will have

$$\delta U_2 = k_{\mathrm{B}} T \Big(\ln \frac{\Omega C}{1+\Omega C} + \frac{1}{1+\Omega C} + \frac{\chi}{(1+\Omega C)^2} \Big) \delta C. \tag{A3}$$

With Eqs. (3) and (A3), we will have

$$\delta U_2 = \frac{k_{\mathrm{B}} T}{\Omega} \Big(\ln \Big(1 - \frac{1}{\lambda_1\lambda_2\lambda_3} \Big) + \frac{1}{\lambda_1\lambda_2\lambda_3} + \frac{\chi}{\lambda_1^2\lambda_2^2\lambda_3^2} \Big) (\lambda_2\lambda_3\delta\lambda_1 + \lambda_1\lambda_3\delta\lambda_2 + \lambda_1\lambda_2\delta\lambda_3). \tag{A4}$$

With Eqs. (8), (9), (A1), and (A4), we will obtain Eq. (12).

(II) The constitutive theory is consistent with the second law of the thermodynamics

Based on the first law of thermodynamics,

$$W = u + Q, \tag{A5}$$

where W is the work done together by the chemical potential of the water and by the applied force, and Q is the heat produced by the friction during chain segments sliding. There exist six independent

variables in the system, including λ_1, λ_2, λ_3, Δ_{12}, Δ_{13}, and Δ_{23}, where Δ_{12} denotes the change in the contour length from the chain segment 1 to the chain segment 2 within the RVE, Δ_{13} denotes the change in the contour length from the chain segment 1 to the chain segment 3 within the RVE, and Δ_{23} denotes the change in the contour length from the chain segment 2 to the chain segment 3 within the RVE.

With Eq. (6), the variation of W is given by

$$\delta W = \Big(\sigma_1 + \frac{\mu}{\Omega}\Big) l_0^3 \lambda_2 \lambda_3 \delta\lambda_1 + \Big(\sigma_2 + \frac{\mu}{\Omega}\Big) l_0^3 \lambda_3 \lambda_1 \delta\lambda_2 + \Big(\sigma_3 + \frac{\mu}{\Omega}\Big) l_0^3 \lambda_1 \lambda_2 \delta\lambda_3. \tag{A6}$$

The variation of u is given by

$$\begin{aligned}\delta u = {} & \frac{\partial u}{\partial \lambda_1}\delta\lambda_1 + \frac{\partial u}{\partial \lambda_2}\delta\lambda_2 + \frac{\partial u}{\partial \lambda_3}\delta\lambda_3 + \Big(\frac{\partial u}{\partial \overline{L}_{\mathrm{C2}}} - \frac{\partial u}{\partial \overline{L}_{\mathrm{C1}}}\Big)\delta\Delta_{12} \\ & + \Big(\frac{\partial u}{\partial \overline{L}_{\mathrm{C3}}} - \frac{\partial u}{\partial \overline{L}_{\mathrm{C1}}}\Big)\delta\Delta_{13} + \Big(\frac{\partial u}{\partial \overline{L}_{\mathrm{C3}}} - \frac{\partial u}{\partial \overline{L}_{\mathrm{C2}}}\Big)\delta\Delta_{23}.\end{aligned} \tag{A7}$$

The variation of Q is given by

$$\delta Q = \frac{\partial Q}{\partial \Delta_{12}}\delta\Delta_{12} + \frac{\partial Q}{\partial \Delta_{13}}\delta\Delta_{13} + \frac{\partial Q}{\partial \Delta_{23}}\delta\Delta_{23}. \tag{A8}$$

Considering that $\delta\lambda_1$, $\delta\lambda_2$, and $\delta\lambda_3$ are arbitrary and independent variables, we will get the exact form as Eq. (8).

Considering that $\delta\Delta_{12}$, $\delta\Delta_{13}$, and $\delta\Delta_{23}$ are arbitrary and independent variables, we will have

$$\begin{cases} \dfrac{\partial u}{\partial \overline{L}_{\mathrm{C1}}} - \dfrac{\partial u}{\partial \overline{L}_{\mathrm{C2}}} = \dfrac{\partial Q}{\partial \Delta_{12}}, \\ \dfrac{\partial u}{\partial \overline{L}_{\mathrm{C1}}} - \dfrac{\partial u}{\partial \overline{L}_{\mathrm{C3}}} = \dfrac{\partial Q}{\partial \Delta_{13}}, \\ \dfrac{\partial u}{\partial \overline{L}_{\mathrm{C2}}} - \dfrac{\partial u}{\partial \overline{L}_{\mathrm{C3}}} = \dfrac{\partial Q}{\partial \Delta_{23}}. \end{cases} \tag{A9}$$

With Eqs. (4), (10), and (A9), we will obtain

$$\begin{cases} \dfrac{\partial Q}{\partial \Delta_{12}} = \dfrac{N_0}{3}\dfrac{x_2}{\overline{L}_{\mathrm{C2}}}F_2 - \dfrac{N_0}{3}\dfrac{x_1}{\overline{L}_{\mathrm{C1}}}F_1, \\ \dfrac{\partial Q}{\partial \Delta_{13}} = \dfrac{N_0}{3}\dfrac{x_3}{\overline{L}_{\mathrm{C3}}}F_3 - \dfrac{N_0}{3}\dfrac{x_1}{\overline{L}_{\mathrm{C1}}}F_1, \\ \dfrac{\partial Q}{\partial \Delta_{23}} = \dfrac{N_0}{3}\dfrac{x_3}{\overline{L}_{\mathrm{C3}}}F_3 - \dfrac{N_0}{3}\dfrac{x_2}{\overline{L}_{\mathrm{C2}}}F_2, \end{cases} \tag{A10}$$

where x_1, x_2, and x_3 are the displacements of one end with respect to the other end of three chain segments within the RVE.

With the specification of Eq. (13), we will have

$$\begin{cases} \dot{\Delta}_{12} = \dfrac{F_2 - F_1}{\eta}, \\ \dot{\Delta}_{13} = \dfrac{F_3 - F_1}{\eta}, \\ \dot{\Delta}_{23} = \dfrac{F_3 - F_2}{\eta}. \end{cases} \tag{A11}$$

With Eqs. (A10) and (A11), we have

$$\begin{aligned}\dot{Q} = {} & \frac{\partial Q}{\partial \Delta_{12}}\dot{\Delta}_{12} + \frac{\partial Q}{\partial \Delta_{13}}\dot{\Delta}_{13} + \frac{\partial Q}{\partial \Delta_{23}}\dot{\Delta}_{23} \\ = {} & \frac{N_0}{3}\Big(\frac{x_1}{\overline{L}_{\mathrm{C1}}}F_1 - \frac{x_2}{\overline{L}_{\mathrm{C2}}}F_2\Big)\frac{F_1 - F_2}{\eta} + \frac{N_0}{3}\Big(\frac{x_1}{\overline{L}_{\mathrm{C1}}}F_1 - \frac{x_3}{\overline{L}_{\mathrm{C3}}}F_3\Big)\frac{F_1 - F_3}{\eta} \\ & + \frac{N_0}{3}\Big(\frac{x_2}{\overline{L}_{\mathrm{C2}}}F_2 - \frac{x_3}{\overline{L}_{\mathrm{C3}}}F_3\Big)\frac{F_2 - F_3}{\eta}.\end{aligned} \tag{A12}$$

Noting that F monotonously increases with $\frac{x}{L_{\mathrm{C}}}$ in Eq. (4), we can show that $\dot{Q} \geqslant 0$. With $\mathrm{d}S = \frac{\mathrm{d}Q}{T}$, where S denotes the entropy of the system, $\mathrm{d}S \geqslant 0$, the second law of thermodynamics will be satisfied.